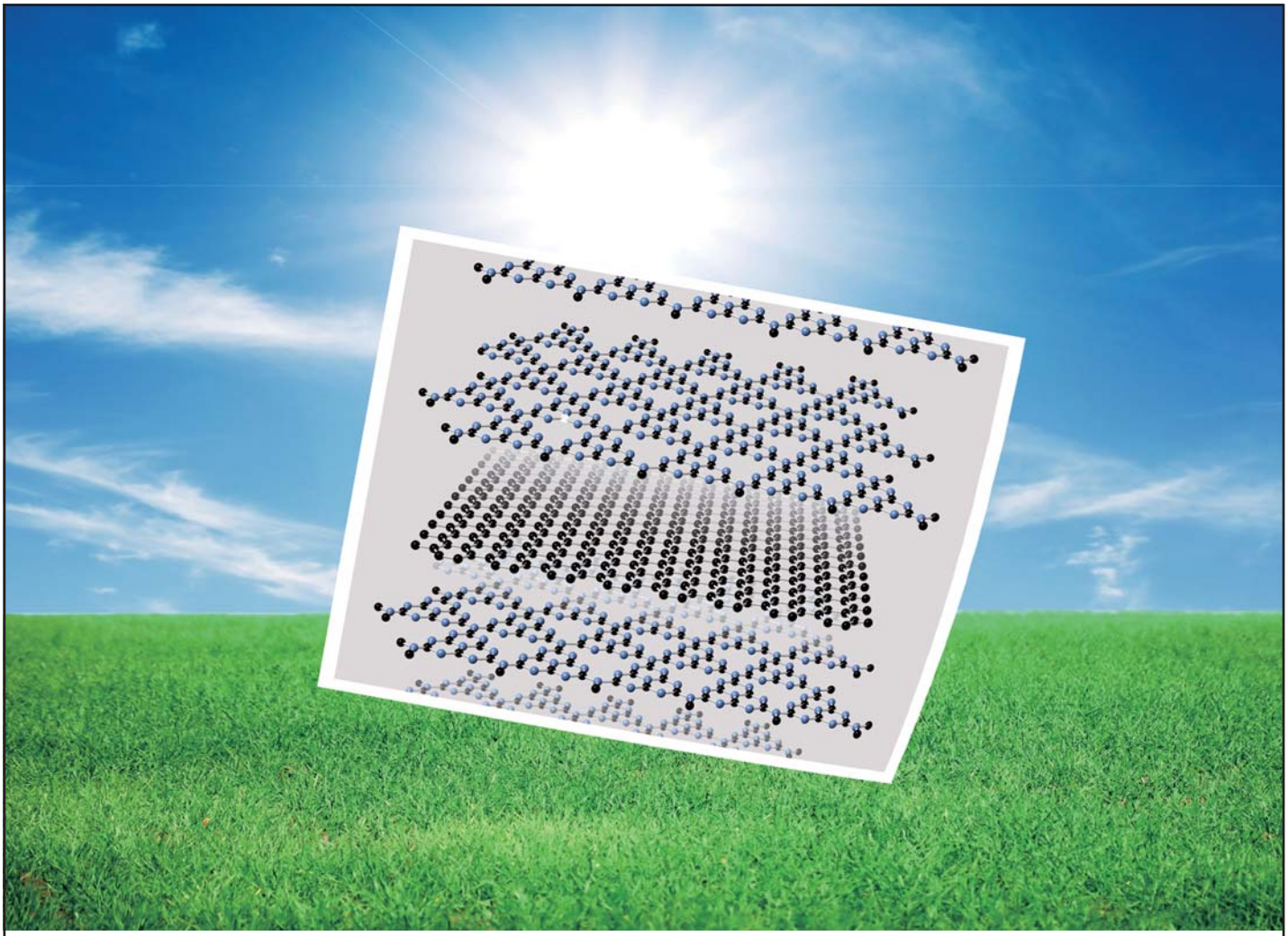

Showcasing research from Zhang *et al* at National Institute for Materials Science, Japan and Changchun Institute of Applied Chemistry, China.

Title: Non-covalent doping of graphitic carbon nitride polymer with graphene: controlled electronic structure and enhanced optoelectronic conversion

Not merely interesting in itself, graphene was used as an interesting dopant for another semiconductor. After intercalation with a few graphene layers via π– π stacking interaction, the band-structure of graphitic carbon nitride was well modulated between more "n-type" and more "p-type".

As featured in:

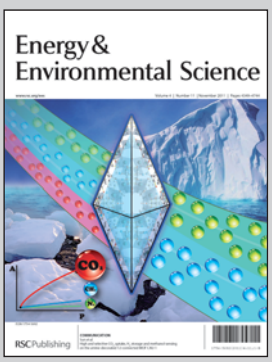

See Zhang *et al.*,
Energy Environ. Sci., 2004, **4**, 4517.

RSC Publishing

www.rsc.org/ees

Registered Charity Number 207890

Energy & Environmental Science

Dynamic Article Links

Cite this: *Energy Environ. Sci.*, 2011, **4**, 4517

www.rsc.org/ees

COMMUNICATION

Non-covalent doping of graphitic carbon nitride polymer with graphene: controlled electronic structure and enhanced optoelectronic conversion†

Yuanjian Zhang,*[a] Toshiyuki Mori,[a] Li Niu*[b] and Jinhua Ye[a]

Received 2nd April 2011, Accepted 8th July 2011
DOI: 10.1039/c1ee01400e

By union of graphitic carbon nitride polymer with reduced graphene oxide (rGO, ≤1 wt%) *via* π–π stacking interaction, the band structure of carbon nitride could be well modulated. As a result, a significant increase of photocurrent was observed (*e.g.*, when biased at 0.4 V *vs.* Ag/AgCl, the anodic photocurrent became 300% higher after doping). Not merely interesting in itself, graphene was also used as a general dopant for semiconductors in band-structure engineering.

As one of the natural elements, carbon has already created a disproportionate amount of curiosities in science. Among various carbon allotropes, graphene has attracted much attention and revealed interesting applications since 2004.[1] Especially, the unique electric, optical and mechanical properties are of great interest, because of its one-atom thick, two-dimensional layer of sp^2-bonded carbon structure (Fig. 1a). Among the most spectacular physical and chemical properties, graphene was found to be an electron collector and transporter, which may be used to boost performances of various energy conversion and storage devices such as photovoltaic devices,[2] supercapacitors[3] and Li-ion batteries,[4] or to be a dispersible carrier for catalysts[5] and a template for chemical reactions.[6] Additionally, many efforts have also been devoted to modifying the electronic structure of graphene by physical cutting[7] or chemical doping.[8] However, graphene has seldom been used as a dopant with the purpose of manipulating the electronic structure of other semiconductors.

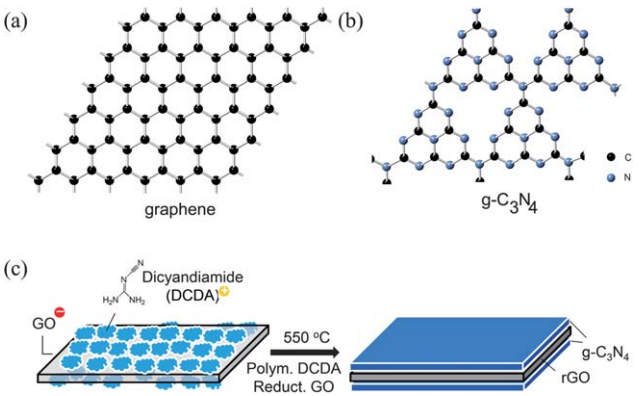

Fig. 1 Idealized motif of graphene (a) and graphitic C_3N_4 (g-C_3N_4) sheet (b). Brief procedure of preparing reduced graphene oxide (rGO)-intercalated g-C_3N_4 (c).

[a]*International Center for Young Scientists (ICYS), International Center for Materials Nanoarchitectonics (MANA), National Institute for Materials Science (NIMS), 1-1 Namiki, Tsukuba, 305-0044, Japan. E-mail: ZHANG.Yuanjian@nims.go.jp*
[b]*Engineering Laboratory for Modern Analytical Techniques, c/o State Key Laboratory of Electroanalytical Chemistry, Changchun Institute of Applied Chemistry, Chinese Academy of Sciences, Renming street 5625, Changchun, 130022, P. R. China. E-mail: lniu@ciac.jl.cn*

† Electronic supplementary information (ESI) available: Experimental details, Fig. S1–S9, Tables S1 and S2, and more discussions. See DOI: 10.1039/c1ee01400e

Broader context

Graphene is a fascinating material not only for electronic applications, but also as a dispersible aromatic platform for chemical reactions or as a carrier for catalysts. However, graphene is not merely interesting in itself. Here we show that graphene was used as a dopant for semiconductors in band-structure engineering. Like the union of tetrathiafulvalene (TTF) with tetracyanoquinodimethane (TCNQ) through π–π stacking forming a new molecule, we stacked graphene with its analogue, graphitic carbon nitride (g-C_3N_4) sheet. Our results showed that by doping with reduced graphene oxide (rGO, ≤1 wt%) the band structure of g-C_3N_4 was modulated between more "n-type" and more "p-type". Consequently, a significant increase of either anodic or cathodic photocurrent from g-C_3N_4 was obtained (*e.g.*, when biased at 0.4 V *vs.* Ag/AgCl, the anodic photocurrent was 300% higher after doping). Moreover, the host semiconductors are feasibly extended to other layered semiconductors; therefore, graphene would be promising as a general intercalating dopant. Meanwhile, it also implicated the rational combination of any other two-dimensional materials towards new properties.

As an analogue of graphite, graphitic carbon nitride also possesses a stacked two-dimensional structure, which could be regarded as *N*-substituted graphite in a regular fashion (Fig. 1b shows one idealized structure of graphitic C_3N_4, g-C_3N_4).[9] Very recently, proof-of-concept studies by us and other groups showed organic semiconductors based on graphitic carbon nitride polymers (*C/N ≈ 0.72, a slightly disordered precursor of g-C_3N_4, for simplicity we use g-C_3N_4 as the whole family of compounds*)‡ are promising candidates for applications in optoelectronic conversion,[10] and are used as photocatalysts in water splitting[11] and degradation of organic pollutants.[12] However, the efficiency of bulk g-C_3N_4 in visible light is rather low because it is hindered by the marginal absorption of visible light and grain boundary effects, and, therefore it must be improved. In this sense, chemical doping such as ionic[10a] and covalent[10c,11c,12b,13] functionalization has been exampled to be an effective strategy to modify the electronic structures of g-C_3N_4, and improve its performances.

The motivation for the study came from the union of tetrathiafulvalene (TTF) and tetracyanoquinodimethane (TCNQ) through π–π stacking interaction forming TTF–TCNQ—a distinct charge-transfer complex with metallic electrical conductance.[14] And it intrigued us to consider what happens if g-C_3N_4 sheets and graphene sheets interact *via* a similar π–π stacking interaction. Here we show that by simply intercalating with different concentrations of reduced graphene oxide (rGO, ≤1 wt%) of different oxygen-defects, the flat-band potential of g-C_3N_4 shifted greatly, while the conduction band (CB) and valence band (VB) edge changed little. Thus, the band structure of g-C_3N_4 was well modulated between more "n-type" and more "p-type". Consequently, a significant increase in either anodic or cathodic photocurrent of g-C_3N_4 after doping was observed, measured in a photoelectrochemical cell. For instance, when biased at 0.4 V (*vs.* Ag/AgCl), the anodic photocurrent was 300% higher than that after doping. Complementary to previous ionic[10a] and covalent[10c,11c,12b,13] doping, the third strategy reported here, *i.e.*, non-covalent doping would establish a more comprehensive understanding of the correlations between the chemical doping of g-C_3N_4 and enhanced performances. Therefore, it would be a significant step towards the emerging photovoltaic applications of g-C_3N_4. Meanwhile, it would shed new light for graphene as a general dopant in optoelectronic applications.

Graphene oxide (GO) was selected as the precursor for the rGO dopant, and was prepared from natural graphite flakes using a modified Hummers method.[15] It was because GO could be firstly exfoliated into single sheets (see the AFM image in Fig. S1†), then uniformly mixed with the monomer of g-C_3N_4 (dicyandiamide, DCDA) in water *via* electrostatic interaction, and lastly converted back to graphene by reduction. Accordingly, rGO-doped g-C_3N_4 was briefly prepared by heating the composite of GO and DCDA at 550 °C in air for 4 h, during which, the polycondensation of DCDA was accompanied by the reduction of GO (Fig. 1c and S2†).[16] FT-IR, XPS, UV-vis and Raman studies all gave evidence that the product was indeed rGO-doped g-C_3N_4, which will be discussed below. In contrast, heating GO or even rGO alone under the same condition resulted in a complete decomposition (see TGA curves and more discussion in Fig. S3†). It strongly implicated a reasonable interaction between g-C_3N_4 and rGO. Furthermore, there was no bulk-phase separation of rGO and g-C_3N_4 in the final product, thus g-C_3N_4 could "protect" rGO against oxidation in air during the reaction at 550 °C. For abbreviation, rGO-doped g-C_3N_4 prepared in air is denoted as CNG-*n*-air, *where n is the initial weight ratio of DCDA to GO*. Similarly, the reaction can be performed in argon as well, and the product is named as CNG-*n*-Ar.

In Fig. 2a, FT-IR spectra of all "doped" g-C_3N_4 samples show the typical C–N heterocycle stretches in ~1100 to 1600 cm^{-1} region, which was related to the extended network connection, and the breathing mode of the tri-*s*-triazine units at 800 cm^{-1}. Moreover, as a semiconductor, the characteristic absorption edge of doped g-C_3N_4 around 460 nm was similar to that of pristine g-C_3N_4 (Fig. 2b and S4†). Therefore, the basic framework of the host g-C_3N_4 stayed mostly unchanged after the doping.

Apart from this, FT-IR spectra (Fig. 2a), together with XPS spectra (Fig. S5a†), show that non-sp^2 carbon bonds (*e.g.* C–O, C=O, and O–C=O) of GO almost disappeared after the reaction at 550 °C, indicating the reduction of GO.[17] The formation of rGO in the final product was also proved by the UV-vis spectra (Fig. 2b and S4†), which show gradually increased featureless absorption of rGO between 500 and 800 nm, a typical behavior of graphene.[17] Raman spectra (Fig. S5b†) provided further evidence of the presence of graphene materials in doped g-C_3N_4. For instance, they show the characteristic G band of the sp^2-bonded C–C in rGO-doped g-C_3N_4. Moreover, a more notable 2D peak (another signature of sp^2 C–C) was observed when encapsulated rGO was fully exposed by decomposing g-C_3N_4 (through annealing rGO-doped g-C_3N_4 in N_2 at 1000 °C, see the TGA curve in Fig. S6† and the SEM image in Fig. S7c†, and more discussion in the ESI†). Therefore, all these spectroscopic studies confirmed that GO was almost reduced into rGO and incorporated into the bulk g-C_3N_4.

In general, if two kinds of nanosheets meet, dependent on their interfacial interactions, there are three structural possibilities: bulk-phase separation, disordered 3D network, or layered intercalation. Nevertheless, the aforementioned control TGA measurements (Fig. S3†) had already partially excluded the possibility of bulk-phase separation between rGO and g-C_3N_4. Thus, to achieve more textural information of rGO-doped g-C_3N_4, X-ray powder diffraction (XRD) studies were performed. It was found that all XRD patterns (Fig. 3a) of doped g-C_3N_4 with a tiny concentration of rGO (wt% ≤ 1%, *i.e.* $n \geq 200$) are dominated by a strong peak at 27.4°, almost the same as the typical interlayer-stacking peak (002) of g-C_3N_4, indicating the layered structure of the final product. When the concentration of rGO increased, *e.g.*, in the case of CNG-2.5-Ar, the peak notably decreased to 27.1°, thereby its interlayer distance was larger than that of g-C_3N_4 but still smaller than those of GO ($2\theta = 9.0°$), rGO ($2\theta = 24.4°$) and even graphite ($2\theta = 26.5°$). It not only suggested the intercalation of rGO into g-C_3N_4, but also was indicative of tighter

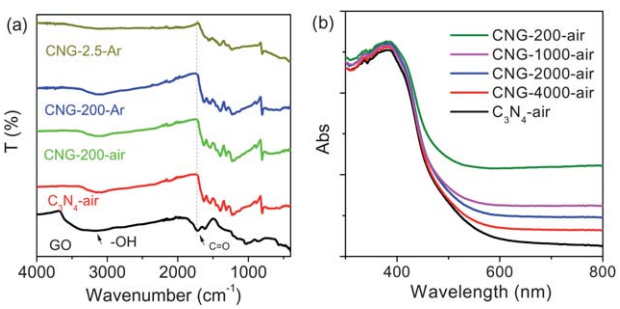

Fig. 2 FT-IR spectra of GO, pristine and rGO-doped g-C_3N_4 prepared in air or Ar (a), and UV-vis absorption spectra of pristine and rGO doped g-C_3N_4 prepared in air (b).

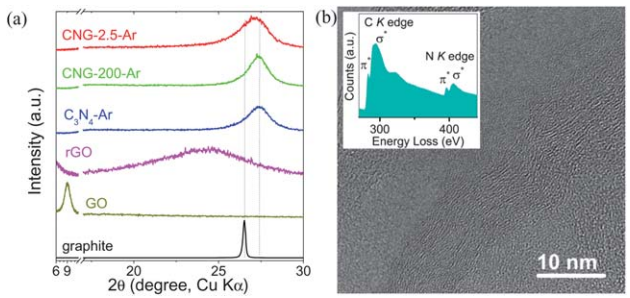

Fig. 3 Normalized XRD patterns of graphite, GO, rGO, C_3N_4-Ar, CNG-200-Ar and CNG-2.5-Ar (a), and a high resolution TEM image of CNG-2.5-Ar (b), inset: electron energy loss spectrum (EELS).

packed layers in CNG-2.5-Ar even than those in graphite. The latter was amazing if considering the rGO percentage was as high as *ca.* 40 wt% (see the following content), thus strongly supported the intercalated layer-structure of rGO-doped g-C_3N_4 (Fig. 1c) for a favourable mixing enthalpy. Otherwise, if a disordered 3D network was formed instead, the average interlayer distance should at least be larger than that of graphite.

Complementarily, the proposed intercalated layer-structure of rGO-doped g-C_3N_4 was further corroborated by scanning electronic microscopy (SEM) and transmission electronic microscopy (TEM) studies. Since it was difficult to distinguish tiny rGO from g-C_3N_4, heavily doped g-C_3N_4, *i.e.* CNG-2.5-Ar, was investigated. As shown in Fig. S7a†, CNG-2.5-Ar had similar slate-like texture at edges like pristine g-C_3N_4 (Fig. S7b†). In addition, no bulk-phase separation between rGO and g-C_3N_4 was observable by SEM measurements accompanied by energy-dispersive X-ray spectra (EDX). The high resolution TEM image in Fig. 3b illustrated the ordered parallel lattice with an inter-planar distance of *ca.* 0.33 nm, which was in agreement with the XRD result. Moreover, the electron energy loss spectrum (EELS) confirmed that these C and N atoms were sp^2-bonded by the presence of 1s → π* transition for both of C and N *K* edges.[18] In addition, the EELS quantification shows rGO wt% ≈ 40%, indicating the above observed layer-structure consisted of both rGO and g-C_3N_4 nanosheets. Therefore, rGO-doped g-C_3N_4 was prepared by simply blending of GO and DCDA and co-thermal treatment at 550 °C, and the current available characterizations indicated that the intercalated layer-structure of rGO-doped g-C_3N_4 was most presumable.

Nevertheless, it was noticed that there were still a few oxygen-defects in rGO-doped g-C_3N_4, which were hard to remove completely.[19] One effect of these oxygen-defects was that they would in turn induce a domino-like self-decomposition of the whole rGO-doped g-C_3N_4 during the reaction at 550 °C in air (Fig. S3c†).[20] For example, when the content of initial GO increased to $n = 10$, both GO and DCDA decomposed, and no product could be obtained finally. However, this self-decomposition effect due to the oxygen-defects could be largely eliminated by performing the reaction in Ar, for instance, even with a higher content of GO (*e.g.* $n = 2.5$). In other words, we could control not only the percentage of rGO, but also the concentration of oxygen-defects in the final rGO-doped g-C_3N_4 (Table S1†). It is well-known that the oxygen-defects would distort the ideal two-dimensional structure of graphene. In this context, these oxygen defects were expected to affect the π–π interaction between rGO and g-C_3N_4, which could consequently influence the electronic structure of g-C_3N_4. This supposition was firstly supported by the Brunauer–Emmett–Teller (BET) surface area measurements. Table S2† shows the BET surface area of CNG-*n*-air was 2–4 times of that of CNG-*n*-Ar with the same amount of rGO, and it significantly increased when the concentration of rGO became higher, while that of CNG-*n*-Ar almost remained constant (*ca.* 6 $m^2 g^{-1}$). Considering their particle sizes were similar from SEM observations, the BET results here hinted that CNG-*n*-Ar was more compact than CNG-*n*-air because of less oxygen-defects and stronger π–π interaction.

A fundamental method used to measure the photoactivity of a new semiconducting material is to utilize a standard photoelectrochemical (PEC) cell configuration in aqueous solution.[21] In this manner, the photocurrent generation from the doped g-C_3N_4 (rGO wt% ≤1%) was investigated in a PEC cell under a chopped simulated sunlight (AM 1.5 G). The black lines in Fig. 4a and b show g-C_3N_4 exhibited an ambipolar behavior under bias voltages ranging from 0.6 to −0.3 V (*vs.* Ag/AgCl). Both cathodic and anodic photocurrents were observed, while an ideal n-type or p-type semiconductor exhibits predominately anodic or cathodic photocurrent, respectively, under the same range of biased potential. It should be noted that in the current PEC cell configuration, the bias voltage was mild, and only visible light was used. The photocurrent was prompt, steady, and reproducible during repeated on/off cycles, and no obvious self-photodegradation of g-C_3N_4 was observed.[10b] Interestingly, dramatic changes in photocurrent generation were observed with different doping concentrations of rGO and with different amounts of oxygen-defects (see representative curves in Fig. 4 and full curves in Fig. S8†). For CNG-*n*-Ar, as denoted by arrows in Fig. 4a, the flat band potentials (E_{fb}), estimated from the photocurrent onset potential,[22] negatively shifted up to 240 mV with the increase of rGO percentage (Fig. 4a and c). As a result, under the same bias potential range, the

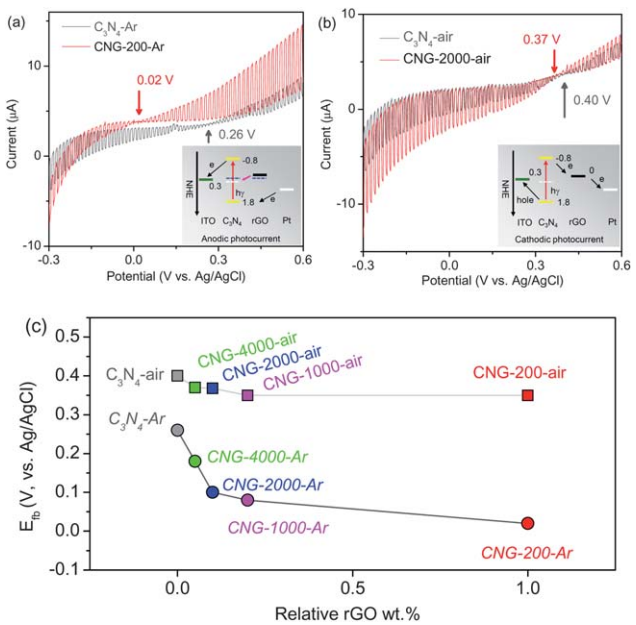

Fig. 4 Photovoltammograms of rGO-doped and pristine g-C_3N_4 synthesized in Ar (a) and in air (b) under chopped visible light (AM 1.5 G) in 0.1 M KCl aqueous solution, scan rate: 10 mV s^{-1}, the arrows indicated the respective photocurrent onset potential, which was used to estimate E_{fb}, inset: proposed mechanisms for anodic and cathodic photocurrent, respectively. The correlation of E_{fb} and relative rGO wt% for various rGO-doped g-C_3N_4 (c).

anodic photocurrent after doping increased remarkably in comparison with that of the pristine g-C_3N_4 and became more apparent than the cathodic photocurrent. For example, when the bias potential was 0.4 V, the anodic photocurrent of CNG-200-Ar was 300% higher than that of pristine g-C_3N_4. In contrast, for CNG-*n*-air, the E_{fb} was almost not changed (≤50 mV, Fig. 4b and c), and the more apparent photocurrent was cathodic. Nevertheless, it was noted that no noticeable difference in morphology was identified among doped or pristine g-C_3N_4 solids (*e.g.* see SEM images in Fig. S7†), and the protocol for the preparation of photoelectrodes (*e.g.* film thickness) was almost the same. Therefore, the grain boundary effect should not dominate such remarkable change of E_{fb} here, but would depress the overall efficiencies of photoelectric conversion, which needs further investigations.

Therefore, in the case of photocurrent generation in PEC cells, CNG-*n*-Ar was more like n-type semiconductor in which anodic photocurrent is more apparent in the present bias potential window, while CNG-*n*-air was more like p-type semiconductor in which cathodic photocurrent is more apparent. Here we proposed a preliminary mechanism (Fig. 4a and b, inset). It was noted that edges of the CB and VB of g-C_3N_4 after the doping did not change (see UV-vis spectra in Fig. 2b and S4†, and valence band XPS spectra in Fig. S9†). In addition, the Fermi-level (E_F) of pristine g-C_3N_4 (approximately in the middle of the band, *i.e.* 0.5 V *vs.* NHE)[10b] was more positive than that of graphene (*ca.* 0 V *vs.* NHE).[2b] Thus, at the idealized interface between rGO and g-C_3N_4, a movement of the charge between their Fermi-levels would occur in order to equilibrate the two phases. Practically, rGO and g-C_3N_4 would stack compactly for CNG-*n*-Ar, because of low concentration of oxygen defects and a strong π–π stacking interaction. Consequently, the electron delocalized from rGO to g-C_3N_4, and a charge-transfer (CT) stacking structure formed. In this respect, CNG-*n*-Ar (rGO wt% ≤1%) seemed to be more than a simple linear combination of rGO and g-C_3N_4, but rather a fused hybrid with new electronic properties. Nevertheless, some distortion should exist if considering the Peierls instability.[14b] As a result, the E_F (approximate to the value of E_{fb} in experiments)[22] of CNG-*n*-Ar moved negatively after the equilibrium, and under the same bias potential window, the anodic photocurrent was more favorable (Fig. 4a, inset). In contrast, for CNG-*n*-air, the π–π stacking interaction between rGO and g-C_3N_4 was weaker, because the higher concentration of oxygen defects made rGO to depart from the ideal two-dimensional structure more notably. Thus, the E_{fb} of CNG-*n*-air was almost constant, but rGO was still capable of accepting and transporting excited electrons under irradiation, resulting in a more apparently cathodic photocurrent under the same bias potential window.

Recently several efforts employing graphene or rGO to boost the photovoltaic performances have been reported. In most cases, graphene or rGO acted as a superior electron collector and transporter,[2] like the way rGO worked in CNG-*n*-air, or as one key component in heterojunction-based devices.[23] However, the finding that rGO could profoundly influence the band structure of host semiconductors *via* a strong π–π electronic interaction, like the case of CNG-*n*-Ar, was seldom reported. Moreover, such electronic interaction could be easily modulated by varying the concentration of rGO and the oxygen-defects in rGO. As an example, it provided a versatile non-covalent way to engineer the flat-band potential of g-C_3N_4, thus either cathodic photocurrent or anodic photocurrent could be remarkably enhanced in a control way. Complementary to previous ionic[10a] and covalent doping,[10c,11c,12b,13] such non-covalent functionalization offered the third strategy. In addition, it is feasible to envisage that the host materials could be extended to other semiconductors, which have strong interactions with graphene, such as layered inorganic semiconducting nanosheets.[24] In fact, small conjugated molecules, such as pyrene and perylene,[8b,25] have already been investigated as dopants to manipulate semiconductors through π–π interactions. And, in a certain sense, graphene is a super conjugated molecule. Therefore, a new application of graphene as a general dopant for other semiconductors may be also fascinating.

It is also worth noting that the graphene prepared here by a chemical method has different morphologies, such as in sizes, shapes, and edges that may have interesting influences on the band structure of g-C_3N_4. It is necessary to deepen the understanding of these effects in experiments, but the synthesis of uniform graphene in bulk quantity is still a challenge, even by a physical route. Thus, a detailed theoretical calculation is underway to assess this specific point.

In summary, rGO was intercalated into bulk g-C_3N_4, a layered organic semiconductor. Owing to the similarity in two-dimensional structure, rGO was expected to possess an effective π–π stacking interaction with g-C_3N_4 that could be well manipulated *via* changing the concentration and the defects (oxygen-groups) of the dopant (rGO). As a result, it provided a controllable non-covalent way to modulate the electronic structure of g-C_3N_4, so that either cathodic photocurrent or anodic photocurrent could be enhanced as required. This control of photocurrent is a significant step towards the emerging photovoltaic applications of g-C_3N_4. Moreover, the present research also suggested the possibility of utilizing graphene as a general dopant for other semiconductors, which might open new vistas of exploring graphene in various optoelectronic applications.

Acknowledgements

This work was supported in part by Grant-in Aid for Young Scientists (B) from the Japan Society for the Promotion of Science (no. 23750177), World Premier International Research Center (WPI) Initiative on Materials Nanoarchitectonics (MANA), MEXT, Japan, and Chinese Academy of Sciences (KGCX2-YW-231), China. We thank Dr Hongqiang Wang (AIST, Japan) and Dr Pavuluri Srinivasu (NIMS) for help in XPS and BET measurements, Dr Takashi Nakanishi, Peng Li (NIMS) and Shizheng Wen (NENU, China) for helpful discussion, and Dr Jesse Williams (NIMS) for language polish.

Notes and references

‡ It should be noted that the C/N ratio of graphitic carbon nitride polymer obtained by heating DCDA at 550 °C was ~0.72, *i.e.*, it was *not* perfectly fully condensed g-C_3N_4 (Fig. 1b). Although g-C_3N_4 with the optimized structure depicted in Fig. 1b has not been prepared in experiments up to now, the as-prepared non-fully condensed polymeric carbon nitride has already found promising applications in energy conversion as a unique organic semiconductor.

1 (*a*) A. K. Geim and K. S. Novoselov, *Nat. Mater.*, 2007, **6**, 183–191; (*b*) Y. Zhu, S. Murali, W. Cai, X. Li, J. W. Suk, J. R. Potts and R. S. Ruoff, *Adv. Mater.*, 2010, **22**, 3906–3924; (*c*) K. P. Loh, Q. L. Bao, G. Eda and M. Chhowalla, *Nat. Chem.*, 2011, **2**, 1015–1024; (*d*) J. Wu, W. Pisula and K. Müllen, *Chem. Rev.*, 2007, **107**, 718–747.

2 (*a*) G. Eda, G. Fanchini and M. Chhowalla, *Nat. Nanotechnol.*, 2008, **3**, 270–274; (*b*) Z. Liu, Q. Liu, Y. Huang, Y. Ma, S. Yin, X. Zhang, W. Sun and Y. Chen, *Adv. Mater.*, 2008, **20**, 3924–3930; (*c*) Y. H. Ng, A. Iwase, A. Kudo and R. Amal, *J. Phys. Chem. Lett.*, 2010, **1**, 2607–2612; (*d*) Y. B. Tang, C. S. Lee, J. Xu, Z. T. Liu, Z. H. Chen, Z. B. He, Y. L. Cao, G. D. Yuan, H. S. Song, L. M. Chen, L. B. Luo, H. M. Cheng, W. J. Zhang, I. Bello and S. T. Lee, *ACS Nano*, 2010, **4**, 3482–3488; (*e*) Y. H. Ng, I. V. Lightcap, K. Goodwin, M. Matsumura and P. V. Kamat, *J. Phys. Chem. Lett.*, 2010, **1**, 2222–2227.

3 (*a*) M. D. Stoller, S. Park, Y. Zhu, J. An and R. S. Ruoff, *Nano Lett.*, 2008, **8**, 3498–3502; (*b*) K. Zhang, L. L. Zhang, X. S. Zhao and J. Wu, *Chem. Mater.*, 2010, **22**, 1392–1401.

4 (*a*) D. Wang, D. Choi, J. Li, Z. Yang, Z. Nie, R. Kou, D. Hu, C. Wang, L. V. Saraf, J. Zhang, I. A. Aksay and J. Liu, *ACS Nano*, 2009, **3**, 907–914; (*b*) G. Zhou, D.-W. Wang, F. Li, L. Zhang, N. Li, Z.-S. Wu, L. Wen, G. Q. Lu and H.-M. Cheng, *Chem. Mater.*, 2010, **22**, 5306–5313.

5 (*a*) E. Yoo, T. Okata, T. Akita, M. Kohyama, J. Nakamura and I. Honma, *Nano Lett.*, 2009, **9**, 2255–2259; (*b*) I. V. Lightcap, T. H. Kosel and P. V. Kamat, *Nano Lett.*, 2010, **10**, 577–583.

6 (*a*) S. B. Yang, X. L. Feng, L. Wang, K. Tang, J. Maier and K. Müllen, *Angew. Chem., Int. Ed.*, 2010, **49**, 4795–4799; (*b*) M. Jahan, Q. Bao, J.-X. Yang and K. P. Loh, *J. Am. Chem. Soc.*, 2010, **132**, 14487–14495.

7 D. V. Kosynkin, A. L. Higginbotham, A. Sinitskii, J. R. Lomeda, A. Dimiev, B. K. Price and J. M. Tour, *Nature*, 2009, **458**, 872–U875.

8 (*a*) X. Li, H. Wang, J. T. Robinson, H. Sanchez, G. Diankov and H. Dai, *J. Am. Chem. Soc.*, 2009, **131**, 15939–15944; (*b*) X. Dong, D. Fu, W. Fang, Y. Shi, P. Chen and L. J. Li, *Small*, 2009, **5**, 1422–1426.

9 (*a*) E. Kroke and M. Schwarz, *Coord. Chem. Rev.*, 2004, **248**, 493–532; (*b*) A. Thomas, A. Fischer, F. Goettmann, M. Antonietti, J.-O. Müller, R. Schlögl and J. M. Carlsson, *J. Mater. Chem.*, 2008, **18**, 4893–4908; (*c*) B. V. Lotsch, M. Doblinger, J. Sehnert, L. Seyfarth, J. Senker, O. Oeckler and W. Schnick, *Chem.–Eur. J.*, 2007, **13**, 4969–4980; (*d*) J. R. Holst and E. G. Gillan, *J. Am. Chem. Soc.*, 2008, **130**, 7373–7379.

10 (*a*) Y. J. Zhang, A. Thomas, M. Antonietti and X. C. Wang, *J. Am. Chem. Soc.*, 2009, **131**, 50–51; (*b*) Y. J. Zhang and M. Antonietti, *Chem.–Asian J.*, 2010, **5**, 1307–1311; (*c*) Y. J. Zhang, T. Mori, J. H. Ye and M. Antonietti, *J. Am. Chem. Soc.*, 2010, **132**, 6294–6295.

11 (*a*) X. C. Wang, K. Maeda, A. Thomas, K. Takanabe, G. Xin, J. M. Carlsson, K. Domen and M. Antonietti, *Nat. Mater.*, 2009, **8**, 76–80; (*b*) K. Maeda, X. Wang, Y. Nishihara, D. Lu, M. Antonietti and K. Domen, *J. Phys. Chem. C*, 2009, **113**, 4940–4947; (*c*) G. Liu, P. Niu, C. H. Sun, S. C. Smith, Z. G. Chen, G. Q. Lu and H. M. Cheng, *J. Am. Chem. Soc.*, 2010, **132**, 11642–11648.

12 (*a*) S. C. Yan, Z. S. Li and Z. G. Zou, *Langmuir*, 2009, **25**, 10397–10401; (*b*) S. C. Yan, Z. S. Li and Z. G. Zou, *Langmuir*, 2010, **26**, 3894–3901.

13 J. S. Zhang, X. F. Chen, K. Takanabe, K. Maeda, K. Domen, J. D. Epping, X. Z. Fu, M. Antonietti and X. C. Wang, *Angew. Chem., Int. Ed.*, 2010, **49**, 441–444.

14 (*a*) P. W. Anderson, P. A. Lee and M. Saitoh, *Solid State Commun.*, 1973, **13**, 595–598; (*b*) L. B. Coleman, M. J. Cohen, D. J. Sandman, F. G. Yamagishi, A. F. Garito and A. J. Heeger, *Solid State Commun.*, 1993, **88**, 989–995.

15 W. S. Hummers and R. E. Offeman, *J. Am. Chem. Soc.*, 1958, **80**, 1339.

16 Y. Wang, X. C. Wang, M. Antonietti and Y. J. Zhang, *ChemSusChem*, 2010, **3**, 435–439.

17 D. Li, M. B. Muller, S. Gilje, R. B. Kaner and G. G. Wallace, *Nat. Nanotechnol.*, 2008, **3**, 101–105.

18 Z. Zhang, K. Leinenweber, M. Bauer, L. A. J. Garvie, P. F. McMillan and G. H. Wolf, *J. Am. Chem. Soc.*, 2001, **123**, 7788–7796.

19 A. Bagri, C. Mattevi, M. Acik, Y. J. Chabal, M. Chhowalla and V. B. Shenoy, *Nat. Chem.*, 2010, **2**, 581–587.

20 F. Kim, J. Luo, R. Cruz-Silva, L. J. Cote, K. Sohn and J. Huang, *Adv. Funct. Mater.*, 2010, **20**, 2867–2873.

21 M. Sharon, in *Encyclopedia of Electrochemistry*, ed. A. J. Bard, M. Stratmann and S. Licht, Wiley-VCH, 2002, p. 287.

22 (*a*) N. Sakai, Y. Ebina, K. Takada and T. Sasaki, *J. Am. Chem. Soc.*, 2004, **126**, 5851–5858; (*b*) M. A. Alpuche-Aviles and Y. Y. Wu, *J. Am. Chem. Soc.*, 2009, **131**, 3216–3224.

23 (*a*) H. Yu, S. Chen, X. Fan, X. Quan, H. Zhao, X. Li and Y. Zhang, *Angew. Chem., Int. Ed.*, 2010, **49**, 5106–5109; (*b*) C. Chen, W. M. Cai, M. C. Long, B. X. Zhou, Y. H. Wu, D. Y. Wu and Y. J. Feng, *ACS Nano*, 2010, **4**, 6425–6432.

24 R. E. Schaak and T. E. Mallouk, *Chem. Mater.*, 2002, **14**, 1455–1471.

25 C. Ehli, C. Oelsner, D. M. Guldi, A. Mateo-Alonso, M. Prato, C. Schmidt, C. Backes, F. Hauke and A. Hirsch, *Nat. Chem.*, 2009, **1**, 243–249.